

# On the universality of void density profiles

E. Ricciardelli<sup>1\*</sup>, V. Quilis<sup>1</sup>, J. Varela<sup>2</sup>

<sup>1</sup>*Departament d'Astronomia i Astrofísica, Universitat de València, c/ Dr. Moliner 50, E-46100 - Burjassot, Valencia, Spain*

<sup>2</sup>*Centro de Estudios de Física del Cosmos de Aragón (CEFCA), Plaza San Juan 1, 44001 Teruel, Spain*

Accepted ... Received ...; in original form ...

## ABSTRACT

The massive exploitation of cosmic voids for precision cosmology in the upcoming dark energy experiments, requires a robust understanding of their internal structure, particularly of their density profile. We show that the void density profile is insensitive to the void radius both in a catalogue of observed voids and in voids from a large cosmological simulation. However, the observed and simulated voids display remarkably different profile shapes, with the former having much steeper profiles than the latter. Sparsity can not be the main reason for this discrepancy, as we demonstrate that the profile can be recovered with reasonable accuracy even with very sparse samples of tracers. On the other hand, the observed profile shows a significant dependence on the galaxy sample used to trace the matter distribution. Samples including low-mass galaxies lead to shallower profiles with respect to the samples where only massive galaxies are used, as faint galaxies live closer to the void centre. We argue that galaxies are biased tracers when used to probe the matter distribution within voids.

**Key words:** cosmology: dark matter – cosmology: observations– large-scale structure of Universe – methods: numerical

## 1 INTRODUCTION

Large redshift surveys (York et al. 2000; Colless et al. 2001) and cosmological simulations (Bond, Kofman, & Pogosyan 1996) have revealed that galaxies are distributed inside a cosmic web of walls, filaments and compact clusters. Such a web encloses large underdense regions, referred to as cosmic voids.

Voids were first recognized in the earliest redshift surveys (Gregory & Thompson 1978; Kirshner et al. 1981) as huge empty holes in the galaxy distribution. Nowadays, there is a general consensus in that voids occupy most of the volume of the Universe (Sheth & van de Weygaert 2004; van de Weygaert & Platen 2011; Pan et al. 2012), although there is not yet an agreement on how a genuine void should be defined. Several void finders, which are based on different principles, have been developed. Voids can be identified as spherical regions devoid of galaxies/halos (Gottlöber et al. 2003; Patiri et al. 2006; Varela et al. 2012) or underdense regions, relying on the continuous density field (Plionis & Basilakos 2002; Colberg et al. 2005). More complex algorithms able to capture the complex morphology of voids also exist (Platen, van de Weygaert, & Jones 2007; Neyrinck 2008; Aragon-Calvo & Szalay 2013). Despite their different definition of voids, all these void finders agree in

that voids are extremely empty in the centre and show a sharp increase in the density towards the voids edges (e.g. Colberg et al. 2008).

Voids are believed to originate from negative density fluctuations in the primordial density field. As a result of their underdensity, they are subject to an effective repulsive peculiar gravity, causing their expansion. As a consequence of such an expansion, the matter within the voids evacuates from the interior and accumulates to the boundaries. This leads to void density profiles that evolve towards a reverse top-hat shape (Sheth & van de Weygaert 2004).

A considerable appeal of cosmic voids is their potential in probing cosmological parameters. In particular, being almost devoid of matter, they are extremely sensitive to the nature of dark energy. Indeed, the void ellipticity and its evolution through cosmic time are intimately connected with the local tidal tensor, which, in turn, depends on the dark energy content (Park & Lee 2007; Lavaux & Wandelt 2010; Bos et al. 2012). Voids are also the ideal candidate for probing the expansion history of the Universe through the Alcock-Paczynski test (Alcock & Paczynski 1979), using the average shape of stacked voids (Lavaux & Wandelt 2012; Sutter et al. 2012). The application of such a test to the voids that will be identified in the future Euclid survey (Laureijs et al. 2011) promises to outperform Baryonic Acoustic Oscillation by an order of magnitude in accuracy.

The huge potentiality of voids for precision cos-

\* E-mail: elena.ricciardelli@uv.es

mology requires a robust knowledge of their internal structure, particularly of the density profiles. Works based on cosmological simulations (Colberg et al. 2005; Ricciardelli, Quilis, & Planelles 2013) indicate that the void density profile is universal. As such, it does not depend on void size. On the observational side, the ideal approach to directly constrain the void density profile is through the weak lensing signal of stacked voids (Krause et al. 2013). However, the number of voids available from spectroscopic catalogues is still limited to provide a robust measurement of the signal (Melchior et al. 2013). At present, we can only rely on the galaxy distribution to trace the density within voids (Sutter et al. 2012). Thus, to robustly assess a void model to describe the universal density profile, one also needs to assess the systematic effects arising from the use of the sparse galaxy sampling.

In a previous work (Ricciardelli, Quilis, & Planelles 2013, hereafter RQP13), we have shown, by means of a cosmological simulation, that a two parameters law can be used to fit the density profile of voids of any size, density, morphology and redshift. The best-fit parameters show some dependence on redshift, density, and, on a less degree, morphology, but they are almost independent on the void size, although the limited statistics prevented us to draw robust conclusions. In this work, we want to test this model and its dependence on void radius, against an observed catalogue of voids and a larger simulation, thus dramatically increasing the statistics. In doing so, we provide a robust determination of the systematic effects arising when using the sparse distribution of void galaxies as density tracers.

The structure of the paper is as follows. In Section 2 we introduce our catalogue of observed voids, in Section 3 we describe the simulation used and our void identification procedure. The results on the void density profiles are discussed in Section 4. We conclude in Section 5.

## 2 THE SDSS VOID CATALOGUE

The catalogue of cosmic voids used for the present analysis has been described in Varela et al. (2012). Here we only give a brief description of the main features and the changes with respect to that work.

The galaxy sample used for void identification has been extracted from the New York University Value-Added Galaxy Catalog<sup>1</sup> (NYU-VAGC; Blanton et al. 2005), based on the photometric and spectroscopic catalog of SDSS/DR7<sup>2</sup>, complete down to  $r \sim 17.8$ . These authors also provide stellar masses computed with the code kcorrect (version 4.1.4) following the prescriptions of Blanton & Roweis (2007). Stellar masses have been computed assuming  $h = 1$ . To guarantee the homogeneity of the sample and avoid the detection of spurious voids, a complete catalogue up to redshift 0.12 and down to magnitude  $M_r - 5\log h = -20.17$  has been used. Using this galaxy sample, voids are defined as spherical regions devoid of galaxies. In the original catalogue of Varela et al. (2012) only voids larger than  $10 h^{-1} Mpc$  were considered for the analysis. In this work, in order to

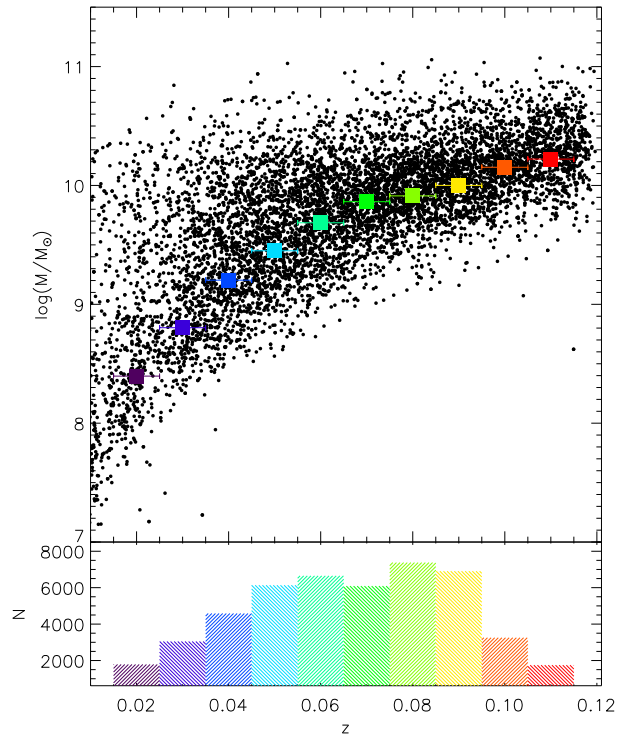


**Figure 1.** Upper panel: void galaxies (black points) in the redshift stellar mass plane. For the sake of clearness only a randomly selected subsample, including 15% of the galaxies, has been plotted. The coloured points indicate the stellar mass threshold adopted for each redshift bin. Lower panel: number of galaxies with redshift less than  $z$  and more massive than the threshold mass at  $z$ .

increase the number of voids, we have extended the original catalogue to include voids down to  $7 h^{-1} Mpc$ . Moreover, we relax the assumption on void overlapping of Varela et al. (2012) and consider as separate voids all overlapping voids whose distance between centers is larger than the radius of the largest void. The final catalogue contains 4453 voids, with radius as large as  $18.7 h^{-1} Mpc$ . We find a total of 44617 void galaxies, which are, by definition, fainter than  $M_r - 5\log h = -20.17$ .

Figure 1 shows how our void galaxies populate the redshift stellar mass plane. For each redshift bin we compute a stellar mass threshold (coloured points), above which the sample can be considered complete. To choose this mass, we have computed the number counts in mass bins and considered the threshold mass as the central mass of the bin having the largest counts.

## 3 VOIDS IN SIMULATIONS

The simulation used in this work has been performed with the hydrodynamical code MASCLET (Quilis 2004). MASCLET couples an Eulerian approach for describing the gaseous component with an N-body scheme for treating the dark-matter, collisionless component. Gas and dark matter are coupled by the gravity solver. To gain spatial and tempo-

<sup>1</sup> <http://sdss.physics.nyu.edu/vagc/>

<sup>2</sup> <http://cas.sdss.org/astrodr7/en>

ral resolution an adaptive mesh refinement (AMR) scheme is implemented.

The numerical simulation was run assuming a spatially flat  $\Lambda$ CDM cosmology, with the following cosmological parameters: matter density parameter,  $\Omega_m = 0.27$ ; cosmological constant,  $\Omega_\Lambda = \Lambda/3H_o^2 = 0.73$ ; baryon density parameter,  $\Omega_b = 0.045$ ; reduced Hubble constant,  $h = H_o/100 \text{ km s}^{-1} \text{ Mpc}^{-1} = 0.71$ ; power spectrum index,  $n_s = 1$ ; and power spectrum normalisation,  $\sigma_8 = 0.8$ .

The initial conditions are set up at  $z = 100$ , using a CDM transfer function from Eisenstein & Hu (1998), for a cube of comoving side length  $512 h^{-1} \text{ Mpc}$ . The computational domain is discretized with  $512^3$  cubical cells. The mass resolution is thus  $\sim 6 \times 10^{10} h^{-1} M_\odot$  and the coarse spatial resolution is  $1 h^{-1} \text{ Mpc}$ .

Following the philosophy of the simulation presented in RQP13, we have designed the simulation to follow the formation and evolution of low-density regions. Contrary to the common practice in AMR simulations, where the high density regions are refined, we use more resolution in low density regions. During the evolution, the regions in the coarse grid are refined based on the local density, when  $\rho/\rho_B < 10$ , being  $\rho$  and  $\rho_B$  the total density and the background density, respectively. The ratio between the cell sizes for a given level ( $l+1$ ) and its parent level ( $l$ ) is, in our AMR implementation,  $\Delta x_{l+1}/\Delta x_l = 1/2$ . Since in this work we are not interested in the study of the void sub-structures and void galaxies, in this simulation we have only used one level of refinement. The best spatial resolution is therefore  $0.5 h^{-1} \text{ Mpc}$ .

Voids are identified in the simulated volume using the void finder algorithm described in RQP13. This algorithm relies on the continuous density field (including dark matter and gas) to identify the low density regions, that we define as voids. It is based on the basic assumptions that the velocity divergence of the gas within the void is always positive (as a result of void expansion) and that the density at the void edges has a sharp increase. Broadly speaking, it performs the following steps. It first marks cells as candidate for being centers of voids when their overdensity is below a threshold limit and the velocity divergence is positive. It then expands these volumes by adding cells on each coordinate directions until one of the conditions that define the void edge is reached. Void edges are reached when the velocity divergence becomes negative or the density gradient exceeds a threshold value. The procedure thus provides the protovoid, the minimum rectangle parallelepiped contained within a void. To build the actual void, protovoids are allowed to merge with each other when the ratio between the overlapping volume and the largest void is within 0.5 and 0.6. The free parameters involved in the procedure have been set by means of extensive tests of the code on a set of Montecarlo mock voids, as well as on the voids in the simulation. We adopt the same reference values as in RQP13. The density and the velocity divergence used are those defined in the base level ( $l=0$ ) grid.

The final sample of simulated voids includes a total of  $\sim 35000$  voids, filling 60% of the simulated volume and with typical overdensity  $\rho/\rho_B = 0.2$ . For the analysis of the density profiles, we restrict the sample only to large voids, with

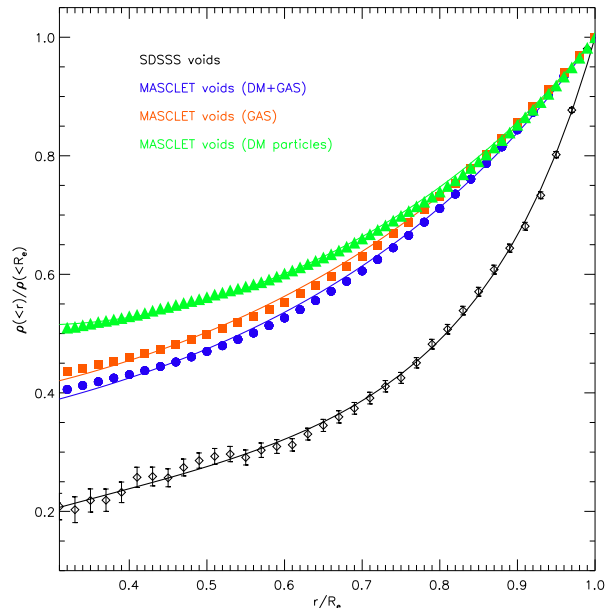


**Figure 2.** Stacked density profiles for all voids larger than  $7 h^{-1} \text{ Mpc}$  identified in the SDSS database (black diamonds) and the best-fit model (black line). As a comparison, the coloured symbols indicate the mean profiles of MASCLET voids larger than  $7 h^{-1} \text{ Mpc}$ . The simulated profiles are computed using various density tracers: total - dark matter plus gas - density field (blue circles), gas density field (orange squares) and dark matter particles (green triangles). The solid coloured lines indicate the best-fits for each curve.  $R_e$  refers to the radius of the voids. For the simulated voids, which have arbitrary shape,  $R_e$  is defined as an equivalent spherical radius, i.e. the radius of the sphere having the same volume of the void. The discrepancy between observed and simulated profiles is addressed in Section 4.2.

effective radius<sup>3</sup>  $R_e > 7 h^{-1} \text{ Mpc}$ . We also exclude voids having too large porosity and ellipticity, as they are the most affected by contamination from non-void regions. We end up with 3186 voids.

## 4 VOID DENSITY PROFILES

To derive the void density profiles for the simulated voids, we can rely on two different tracers: the continuous density field and the dark matter particles. In both cases, we compute the density in spherical apertures, thus discarding the information about void shape. When using the continuous density field, we compute the profiles for the individual voids and then use the bi-weight estimator at any given aperture for getting the stacked profile. We have restricted the analysis of the profiles to  $r \geq 0.3R_e$ , as in the observed voids we can not reach regions at smaller radii, due to the paucity of galaxies. In Fig. 2 we show the profile computed in this way for all simulated voids larger than  $7 h^{-1} \text{ Mpc}$  (blue line).

The stacked profile is fitted by the two-parameters law proposed in RQP13:

<sup>3</sup> The effective radius is defined as the radius of the sphere having the same volume of the void.

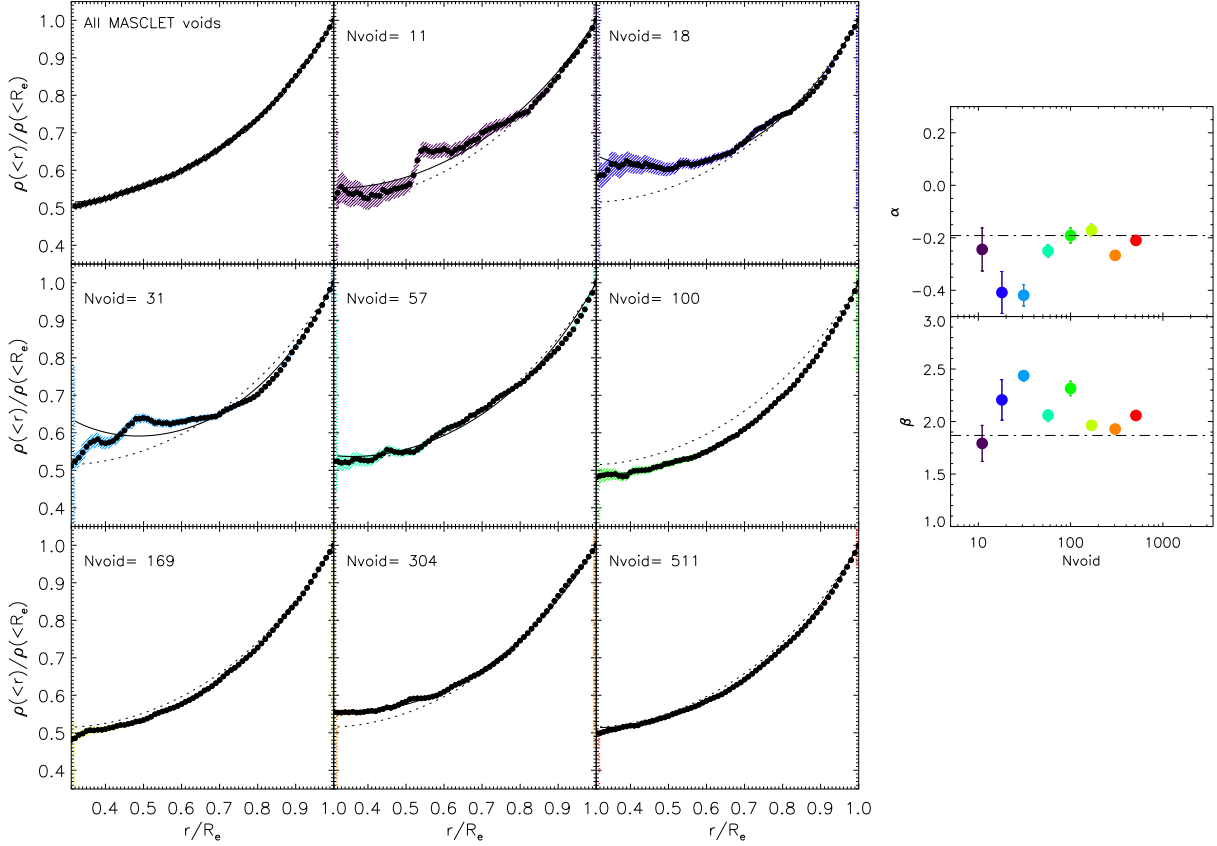


**Figure 3.** Dependence of the simulated void density profiles on the number of voids used in the stacking. The profiles have been computed using the dark matter particles as density tracers. The different panels show the stacked profiles for subsamples of voids extracted from the original sample, populated with an increasing number of voids. The black points indicate the radial value of the stacked void, colored shaded regions show the confidence regions determined by means of a bootstrapping, and the black solid line is the best-fit. The dotted black line reported in all the panels is the best-fit density profile of the stack drawn from the parent sample, when all the voids are included. The dependence of the best-fit parameters on the number of voids used in the stacking is shown in the smaller panels on the right. Error-bars have been computed with the aid of a bootstrapping, see text for further details (Section 4.1).

$$\frac{\rho(<r)}{\rho_e} = \left(\frac{r}{R_e}\right)^\alpha \exp\left[\left(\frac{r}{R_e}\right)^\beta - 1\right] \quad (1)$$

where  $\rho(<r)$  is the density enclosed within the void-centric distance  $r$ ,  $\rho_e$  is the density enclosed within the void effective radius  $R_e$  and  $\alpha$  and  $\beta$  are the best-fit parameters to be obtained from the fit. We notice that in order to avoid a divergent profile for  $r = 0$ , we should require  $\alpha, \beta \geq 0$ . However, since we are applying Eq. 1 to a limited radial range ( $0.3 - 1R_e$ ), we allow  $\alpha$  and  $\beta$  to assume any value. This is particularly useful to quantify the behavior of the inner part of the profile in very different situations. In fact, cases where  $\alpha$  takes negative values do exist, as we show in the following sections. The best-fit parameters that we obtain for the stacked void of Fig. 2 are:  $\alpha = 0.06$  and  $\beta = 1.76$ , compatible with those determined in RQP13, using a sample of smaller voids. We also show the profile when only the density of the baryonic component is considered (orange symbols). As shown in RQP13, the distribution of the gas within low density regions closely follows that of dark matter. Indeed, the density profiles for the two components are in a remarkable agreement and the best-fit parameters for the gas only profile are:  $\alpha = 0.01$  and  $\beta = 1.65$ .

The second method we use, relies on the dark matter

particles within the void regions. In building the stack, we include, for each void, all dark matter particles within the radius limit, and rescale their void-centric distance to the radius of the void hosting the particle. The particles are ranked according to their rescaled distance  $r$ , from the smallest to the largest, and the stacked profile at  $r$  is computed with the following expression:

$$\frac{\rho(<r)}{\rho_e} = \frac{1}{N_{void}} \sum_{i=1}^{N(<r)} \frac{m_i w_i}{(4/3)\pi(rR_{ei})^3 \rho(<R_{ei})} \quad (2)$$

where the summation is intended over all the particles contained within the rescaled radius  $r$ ,  $N_{void}$  is the total number of voids entering in the stack,  $m_i$  is the mass of the  $i$ -th particle,  $R_{ei}$  is the effective radius of the void containing the  $i$ -th particle and  $\rho(<R_{ei})$  is the density enclosed within  $R_{ei}$ , computed with all the particles within the void containing the  $i$ -th particle<sup>4</sup>. The weights  $w_i$  are intended to give low weights to the massive particles falling too close to the void centers, which otherwise would bias the inner profile towards high values. They are defined as:

<sup>4</sup> in the computation of  $\rho(<R_{ei})$  the particle masses are weighted according to Eq. 3 and 4.

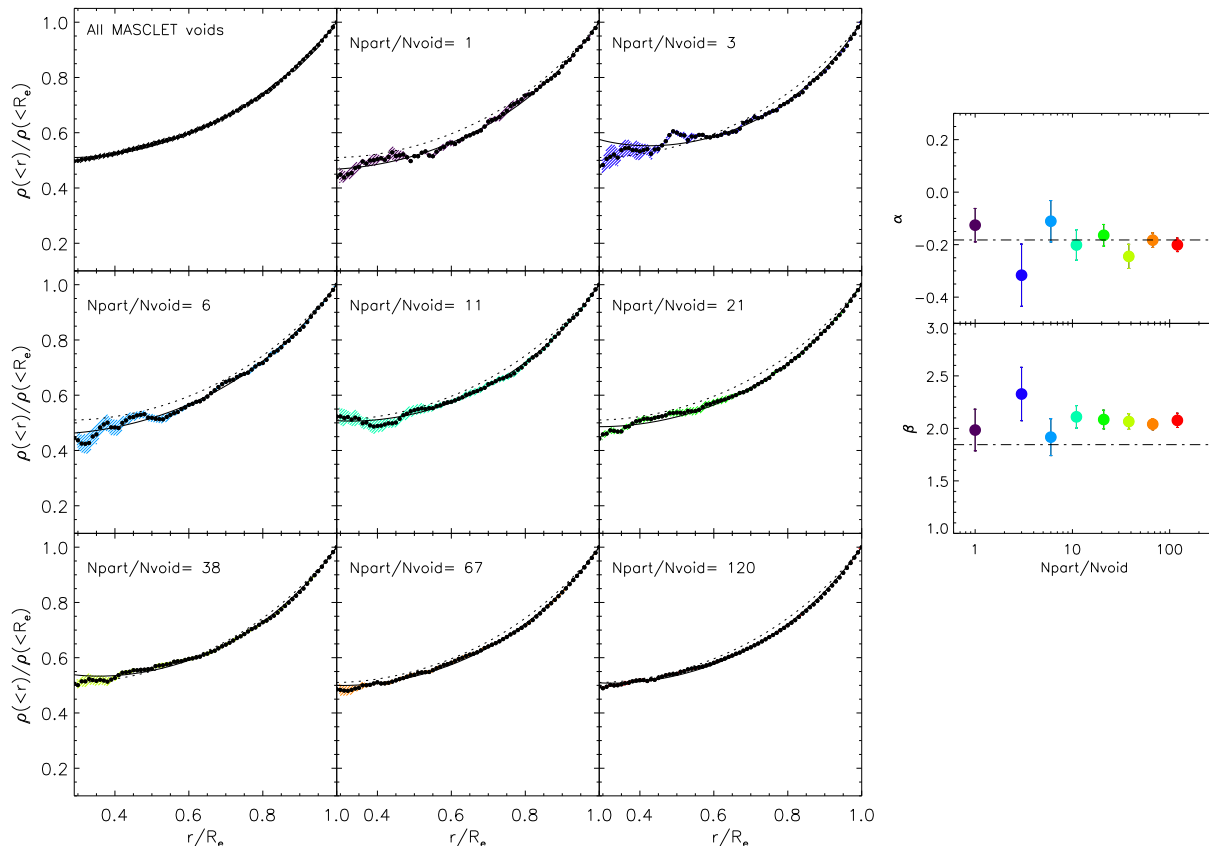


**Figure 4.** Dependence of the simulated void density profiles on the average number of particles per void. The different panels show the stacked profiles for voids populated with an increasing number of particles, extracted from the original sample. As in Fig. 3, the black points indicate the radial value of the stacked void, colored shaded regions show the confidence regions, and the black solid line is the best-fit. The dotted black line reported in all the panels is the best-fit density profile of the stack drawn from the parent sample, when all void particles are included. The dependence of the best-fit parameters on the average number of particles per void is shown in the smaller panels on the right.

$$w_i = (1 - u^2)^2 \quad (3)$$

with:

$$u = \min \left( \left| \frac{(\rho\rho(r) - \overline{\rho\rho})}{N_\sigma\sigma} \right|, 1 \right) \quad (4)$$

being  $\rho\rho = \rho(r)/\rho(R_e)$  the density at the location  $r$ , computed with the mass and location of the  $i$ -th particle, rescaled to the density at the void radius  $\rho(R_e)$ ;  $\overline{\rho\rho}$  is the median density computed with 20 neighbour particles and  $\sigma$  is the median absolute deviation,  $N_\sigma$  is an adjustable parameter, that in our configuration is chosen to be 6<sup>5</sup>. This profile is shown by the green symbols in Fig. 2. It slightly deviates from the one computed with the continuous density field, because the density in the inner part of voids can be seriously affected by the sparsity of the particle distribution. The bi-weight estimator of the individual profiles turns out to be a far more robust method when dealing with very noisy data, such as the density in the very inner

part of voids. However, with dark matter particles we want to adopt the same method that can be used with the SDSS voids, where individual profiles are difficult to be obtained, given the paucity of galaxies living in them.

To derive the void density profiles of the SDSS voids, we need to rely on the luminous galaxies as density tracers. We therefore adopt the same stacking procedure used for stacking the dark matter particles in the simulated voids, by considering all the void galaxies in the parent sample. The observed void density profile is shown in Fig. 2 as black symbols. The functional form expressed in Eq. 1 turns out to be adequate in reproducing also the observed profile, with  $\alpha = 0.50$  and  $\beta = 4.15$ . We find nevertheless that the observed profile is much steeper than the simulated one. Given the close agreement between gas and dark matter density profiles, we can not ascribe such a steepness to a baryonic bias. We investigate the origin of such difference in the following sections.

<sup>5</sup> This weighting scheme is the same adopted in the bi-weight estimator

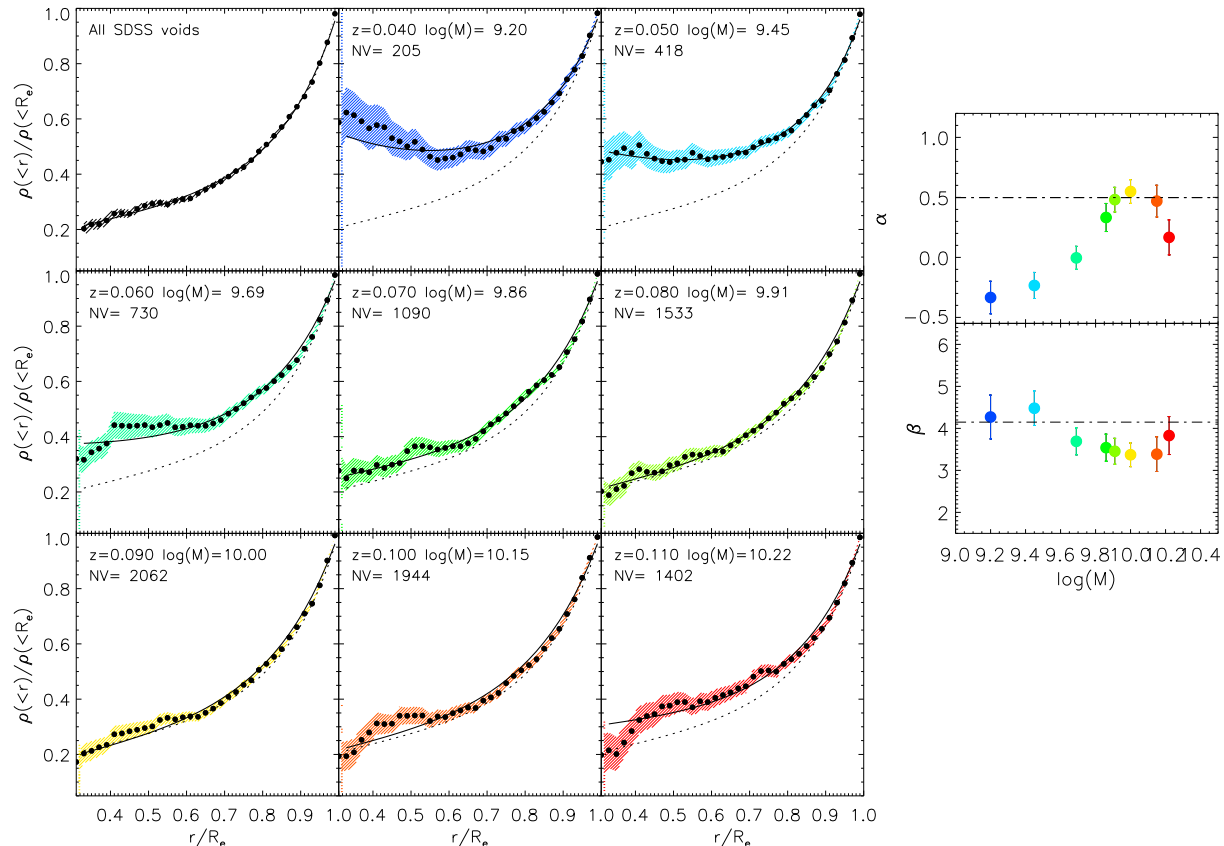


**Figure 5.** Dependence of the observational void density profiles on the choice of the density tracers. Different panels show the density profiles for samples of voids lying at redshift below that indicated and using, as mass tracers, the galaxies more massive than the threshold mass at that redshift. The black points indicate the radial value of the stacked void, colored shaded regions show the confidence regions determined by means of a bootstrapping, and the black solid line is the best fit. The dotted black line reported in all the panels is the best-fit density profiles of the stack drawn from the parent sample (first panel). The dependence of the best-fit parameters on the threshold mass of the galaxies used is shown in the smaller panels on the right.

#### 4.1 Impact of the undersampling

A possible reason for the steepness of the observed density profile could lie in the sparsity of the galaxy distribution. The paucity of galaxies within the observed voids, especially at small void-centric distances, makes difficult to reconstruct the underlying distribution of matter. Indeed, in our catalogue of SDSS voids, the typical number of galaxies populating the voids is 10, and several voids contain only 1-2 galaxies. Therefore, it is important to assess whether the limited statistics or the low density of tracers (either dark matter particles in the simulation or galaxies in the SDSS catalogue) could affect the shape of the void density profile.

In order to test the undersampling, we have used the simulated voids. The undersampling has been tested against both the number of voids used in the stacking and the number of density tracers. Since the resolution of the simulation used for this work is quite modest, we do not find haloes and galaxies within the voids. Therefore, to study the effect of the sparsity of the density tracers we rely on the dark matter particles.

In assessing the effect of the limited statistics, we have randomly extracted subsamples of voids from the parent cat-

alogue. The resulting density profiles are shown in Fig. 3 for subsamples populated with an increasing number of voids. The dependence of the best-fit parameters on the number of voids is shown in the small panels on the right-hand side of Fig. 3. The errors on  $\alpha$  and  $\beta$  have been estimated by means of a bootstrap resampling. For each void subsample, we have generated 100 resamplings with replacement and computed the stacked profile with the relative best-fit values. Their standard deviations give the errors on the measured  $\alpha$  and  $\beta$ . The effect of the limited statistics is to increase the noise in samples where very few voids are stacked, but no systematic effect is observed. As shown by the best-fit parameter panels,  $\alpha$  and  $\beta$  converge to the reference values when at least 100 voids are stacked.

We have also analysed the undersampling effect by computing the profiles with voids populated with an increasing number of dark matter particles. The resulting profiles are shown in Fig. 4. The most important conclusion is that the paucity of tracers does not bias the recovered profiles. As inferred from the behavior of the best-fit parameters of Fig. 4, voids populated with less than 10 particles show some de-

viations from the reference values, because the profiles are particularly noisy, but no systematic effect is observed.

To conclude, we can consider the void density profiles as reliable when more than 100 voids are used in the stack and when they are populated with at least 10 tracers. In the SDSS stack void shown in Fig. 2, both conditions are satisfied, hence we can not ascribe the steepness of the observed profile to undersampling effects.

## 4.2 Impact of the mass tracers

In this section, we study the impact of the sample of galaxies adopted on the resulting density profiles of the observed voids. This is particularly important if one wants to study the void density profiles as a function of the radius of the voids. In fact, the largest voids are more likely observed in the higher redshift bins, as the sampled volume is larger. However, as a consequence of the Malmquist bias, at high redshift only the brightest galaxies are observed (see Fig. 1). Therefore, to compare voids located at different redshifts, we need to know whether the different tracers adopted can affect the resulting profile.

To do this, we have built volume limited samples of galaxies up to a given redshift and complete down to the corresponding threshold mass limit. The redshift and mass limits are those illustrated in Fig. 1. It is worth to emphasize that the choice of the galaxy sample used only affects the recovered density profiles, leaving the sample of voids unchanged. We do not consider samples at  $z < 0.04$  as the number of voids is too limited and the profiles can be affected by undersampling. In Fig. 5 we show the recovered density profiles using the different galaxy samples. The profiles appear to steepen as galaxies at higher redshift and higher stellar mass are used. Interestingly, the profiles traced with the faintest galaxy samples approach the simulated profiles shown in Fig. 2. The steepening is particularly evident in the evolution of  $\alpha$ , that becomes progressively higher as more massive galaxies are concerned. On the other hand,  $\beta$  does not show any clear dependence on the tracers, as the  $\beta$  beta values are just scattered around the reference values.

We exclude redshift evolution as the reason for the profile steepening observed in Fig. 5. Indeed, the evolution of voids in such a narrow redshift range is expected to be negligible and should go in the opposite sense, i.e. steeper profiles at lower redshift (see Figure 9 in RQP13). To understand how the choice of the mass tracers affects the profiles, we show in Fig. 6 the distribution of void-centric distances of void galaxies of different masses. As expected, in all the samples the number of galaxies is extremely scarce in the inner part and then it rapidly grows towards the edge, reaching a maximum at  $r/Re \sim 0.9$ . Low mass galaxies appear to live closer to the void centre, in particular there is an excess of dwarf galaxies at  $r/Re \sim 0.5$ . Conversely, the massive galaxies are more concentrated towards the void edge. A similar effect for the dwarf systems has been also observed by Hoyle, Vogele, & Pan (2012). We argue that the steepness of the observed profile, with respect to the simulated ones, can be explained by the absence of tracers in the innermost regions of the observed voids. It is not clear however whether such absence could be solved by using deeper data or it is just a consequence of the galaxy bias.

We note that a similar comparison of density profiles

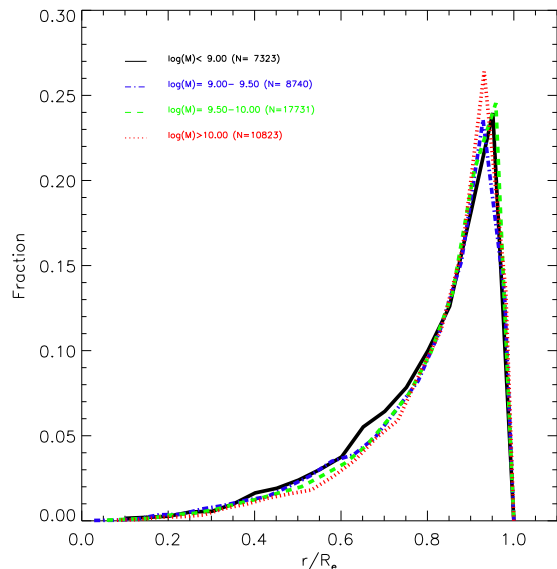


**Figure 6.** Fraction of galaxies as a function of their distance to the void centre, normalized to the void radius. The different lines show galaxies within different mass ranges, as indicated.

measured with different samples of galaxies has been shown by Nadathur & Hotchkiss (2013). They did not find any bias on the profile when considering tracers of different magnitude. However, their galaxy samples are relatively bright ( $Mr < -18.16 + 5\log(h)$ ). Void galaxies in our SDSS catalogue, are, by definition, fainter than  $Mr = -20.17 + 5\log(h)$ , hence allowing us to probe the profiles using also galaxies with very low mass. In fact, if only the highest mass bins were concerned, we would not observe such dependence of the profile on the galaxy mass.

## 4.3 Dependence on void radius

To assess the dependence of the void profiles on the void radius, we use both the observed and simulated voids. In the observed voids, in order not to be affected by the bias described in the previous section, we rely on a homogenous sample of galaxies. We focus on voids located at  $z < 0.08$  and use only galaxies more massive than the threshold mass at this redshift ( $10^{9.9} M_{\odot}$ ) for the stacking. We choose this couple of redshift and mass because is the one maximizing the number of galaxies (see lower panel of Fig. 1). We find 1539 voids and 7725 galaxies satisfying this criteria.

We divide the void sample in equi-populated subsamples, having  $\sim 300$  voids each. This should limit the effect of noise at small radii, shown in Section 4.1. The profiles for different void radii are shown in Fig. 7. All the best-fit parameters,  $\alpha$  and  $\beta$ , fall within 1-2  $\sigma$  of the reference values, derived by fitting the profile of the parent sample at  $z < 0.08$ , without any dependence on the radius. Indeed, the best-fit profile derived for the parent sample (dotted line) is compatible with the profile shape in all the size bins.

We also probe the dependence of void profiles on radius by means of the simulated voids. Fig. 8 shows the density profiles for different void sizes. The density here refers to the total density, including dark matter and gas. A similar

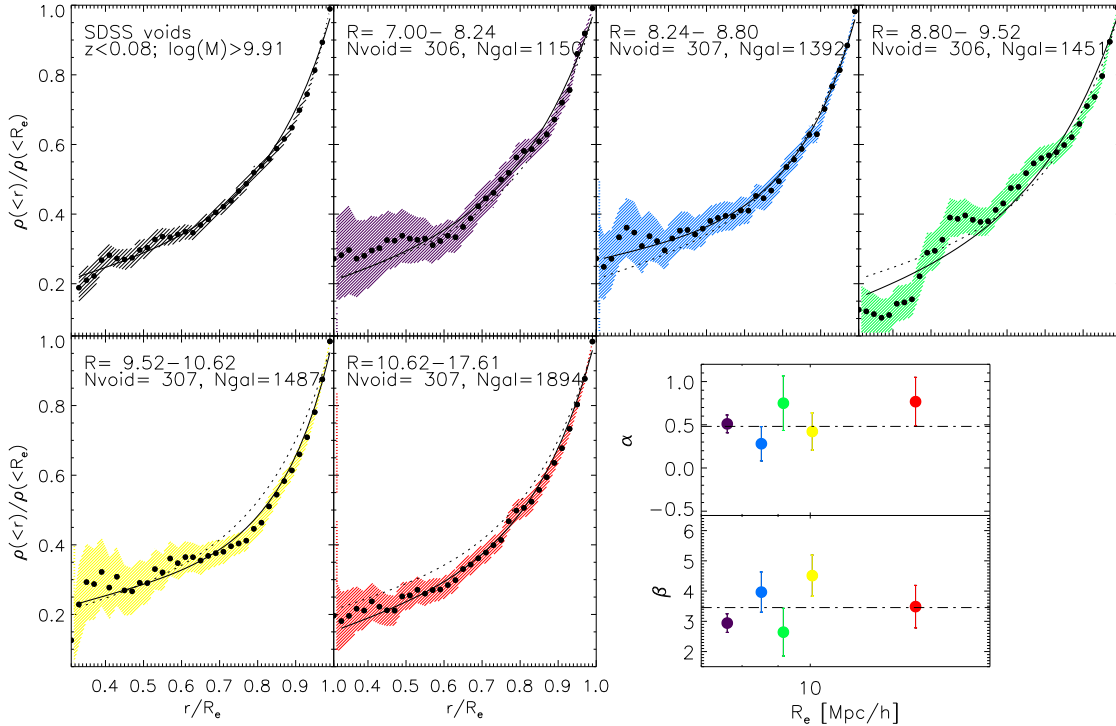


**Figure 7.** Observational void density profiles as a function of void radius. The first panel shows the density profile measured from an homogenous sample of galaxies, with voids lying at  $z < 0.08$  and the mass tracers having stellar mass above  $10^{9.9} M_{\odot}$ . In the other panels, we show the density profiles of voids within different size bins. The black points indicate the radial value of the stacked void, colored shaded regions show the confidence regions determined by means of a bootstrapping, and the black solid line is the best fit. The dotted black line reported in all the panels is the best-fit density profile shown in the first panel. The lower-right panels show the dependence of the best-fit parameters  $\alpha$  and  $\beta$  on void radius.

result is obtained when using the dark matter particles as density tracers. The void sample is divided in different size bins, containing more than 300 voids. Given the large box of the simulation, we are able to probe even the largest voids, having radii up to  $\sim 50 h^{-1} Mpc$ . The profiles of each size bins are in good agreement with that of the parent sample (dotted line). However, in the trend of the best-fit parameters with radius (right-hand upper panels), we observe a positive correlation of  $\alpha$  with  $R_e$  and a negative correlation of  $\beta$  with  $R_e$ . This is due to some degeneracy in the fit, as the two parameters are not completely independent. Therefore, we have fitted the two parameters separately. Hence  $\alpha$  ( $\beta$ ) has been fitted by keeping  $\beta$  ( $\alpha$ ) fixed and equal to its reference value. The results are shown in the lower panels on the right-hand side of Fig. 8. In this case, we do not see any correlation with  $R_e$ . We argue that the profile is independent on the void radius.

We notice that the void density profiles have also been tackled in RQP13, using an analogous simulation as the one presented in this work, though with a much smaller volume. However, in that work the statistics of voids larger than  $8 h^{-1} Mpc$  were too limited, due to the small volume of the simulation, and it was not possible to draw robust conclusions.

## 5 CONCLUSIONS

We have robustly assessed the universality of void density profiles, by means of a catalogue of observed voids and a large cosmological simulation.

The observed void catalogue has been drawn from the SDSS database, and includes spherical voids whose radius is larger than  $7 h^{-1} Mpc$  (Varela et al. 2012). To measure the density profiles in these voids, we rely on the luminous galaxies. As a matter of comparison, we have performed a large cosmological simulation with the code MASCLET, devoted to follow the formation and evolution of the low-density regions. This simulation has been designed to target, with sufficient statistics, voids spanning a wide range of radius. To this aim, we have simulated a large volume, having a co-moving side length of  $512 h^{-1} Mpc$ , with only one level of refinement in the AMR grid, reaching the spatial resolution of  $0.5 h^{-1} Mpc$ . Since this modest resolution does not allow to follow the formation of structures in the simulated box, void galaxies in our simulation do not form. Therefore, we adopt as density tracer the continuous density field or, where a sparse distribution of tracers is needed, the dark matter particles within the void regions.

The void density profiles recovered by means of the observed and simulated voids share the same qualitative shape, showing a significant underdensity in the centre and a sharp



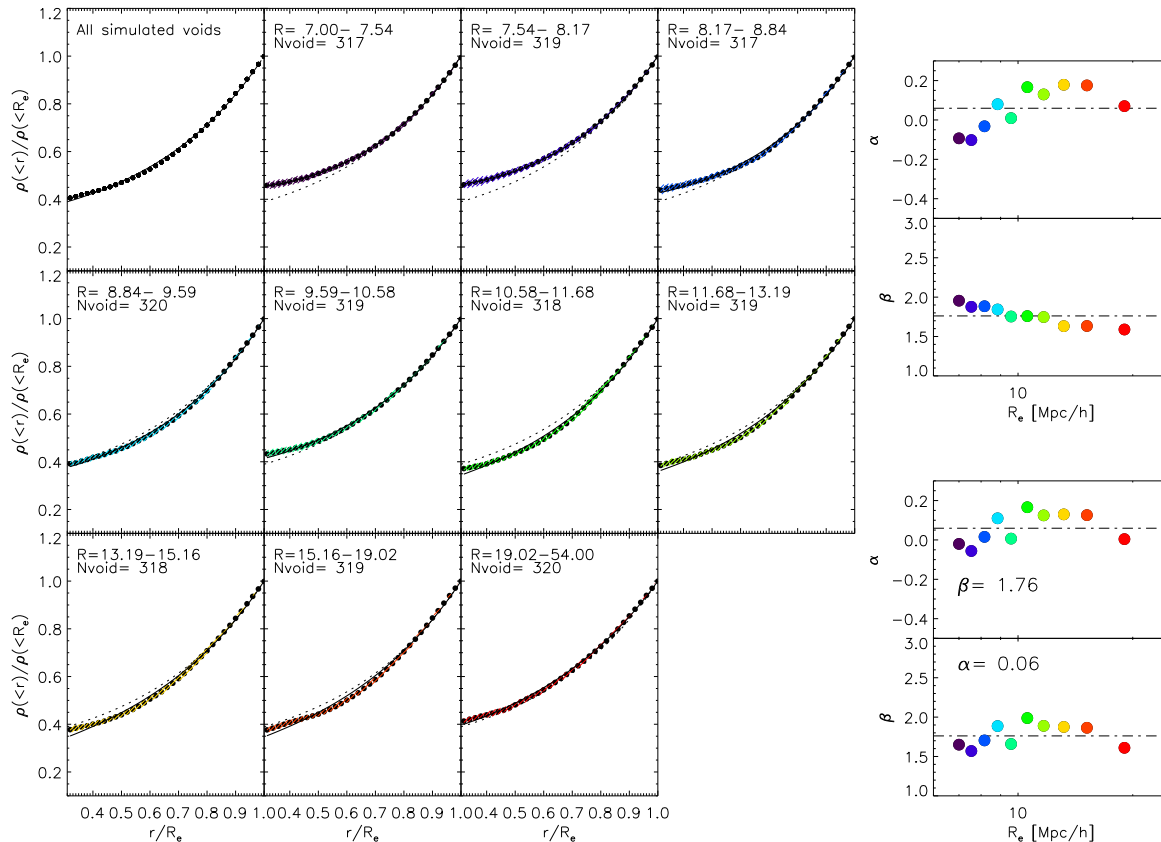


**Figure 8.** Simulated void density profiles as a function of void radius. The first panel shows the mean density profile for all voids larger than  $7h^{-1}Mpc$ , whereas the other panels show the profiles for voids in different size intervals, as indicated. In all panels black symbols indicate the bi-weight mean profile, the coloured shaded regions show the  $1\sigma$  confidence interval and the solid black line stays for the best-fit model. The best-fit profile of the parent sample shown in the first panel is reported, as dotted line, in all the other panels for reference. The dependence of the best-fit parameters on void radius is shown in the smaller panels on the right, in the case of leaving both  $\alpha$  and  $\beta$  free (upper panels) or fixing one of the two to the reference value (lower panels).

density increase approaching the void edges. Both profiles can be well described by the functional form proposed in RQP13. However, the observed profile is significantly steeper than the simulated one.

To figure out the reasons for the steepness of the observed profiles, we have assessed the impact of the number and type of tracers on the resulting density profile. The sparsity of the density tracers has been investigated by means of subsamplings of the simulated voids, populated with an increasing number of particles. We have shown that even in the less populated void samples, the original density profile can be recovered with reasonable accuracy. Stacks built with a limited number of voids or sparsely populated present a significant noise at small radii, but no systematic effect with the number of voids/tracers is observed. The low impact of the sparsity of the tracers on the internal void density profiles has been pointed out also by Sutter et al. (2013), using both dark matter particles and haloes as density tracers.

Nevertheless, we observe that the profile shape can have a significant dependence on the type of galaxies used to trace the matter distribution. Within the observed voids, the density profiles recovered by means of faint samples of galaxies

are shallower than those determined through the brighter galaxies. The reason for that lies in the galaxy mass segregation within voids. In fact, faint galaxies are those living closer to the void centre and, thus, allow to probe the matter distribution even in the innermost part of the voids.

The strong impact of the type of galaxies chosen to trace the density, forces us to use an homogenous sample of galaxies and voids, limited in volume and magnitude, to assess the dependence of the void density profile on the void radius. With such a sample, we have demonstrated the insensitivity of the observed void profile on void radius. Likewise, by using our simulated sample of voids, we do not observe any dependence of the profile shape on the void size, and the same best-fit can correctly describe voids whose size ranges from 7 to  $\sim 50h^{-1}Mpc$ .

Finally, we note that the difference in profile between the observed and simulated voids can not be driven by the different algorithms used to identify voids. Indeed, the density profile of our SDSS stack is very similar to the profile published in Pan et al. (2012), using the same SDSS DR7 dataset, albeit with a completely different void finder. Moreover, our simulated void density profiles are in remark-

able agreement with the simulations of Colberg et al. (2005), where voids are identified through spherical underdensities. Therefore, we argue that the difference between observed and simulated void density profiles is a robust result and is due to the biased tracers used, when relying on the observed galaxies. To corroborate this hypothesis, we definitely need high resolution simulations, capable to follow structure formation in the most rarefied regions of the Universe.

## ACKNOWLEDGEMENTS

We are grateful to Ignacio Trujillo for useful discussions. This work was supported by the Spanish Ministerio de Economía y Competitividad (MINECO, grants AYA2010-21322-C03-01) and the Generalitat Valenciana (grant PROMETEO-2009-103). J.V. did part of the work thanks to a post-doc fellowship from the former Spanish Ministry of Science and Innovation under programs 3I2005 and 3I2406. J.V. also acknowledges the financial support from the FITE (Fondos de Inversin de Teruel) and the Spanish grant AYA2012-30789.

## REFERENCES

- Alcock C., Paczynski B., 1979, *Nature*, 281, 358  
 Aragon-Calvo M. A., Szalay A. S., 2013, *MNRAS*, 428, 3409  
 Blanton M. R., et al., 2005, *AJ*, 129, 2562  
 Blanton M. R., Roweis S., 2007, *AJ*, 133, 734  
 Bond J. R., Kofman L., Pogosyan D., 1996, *Nature*, 380, 603  
 Bos E. G. P., van de Weygaert R., Dolag K., Pettorino V., 2012, *MNRAS*, 426, 440  
 Park D., Lee J., 2007, *PhRvL*, 98, 081301  
 Colberg J. M., et al., 2008, *MNRAS*, 387, 933  
 Colberg J. M., Sheth R. K., Diaferio A., Gao L., Yoshida N., 2005, *MNRAS*, 360, 216  
 Colless M., et al., 2001, *MNRAS*, 328, 1039  
 Eisenstein D.J., Hu W., 1998, *ApJ*, 511, 5  
 Gregory S. A., Thompson L. A., 1978, *ApJ*, 222, 784  
 Gottlöber S., Lokas E. L., Klypin A., Hoffman Y., 2003, *MNRAS*, 344, 715  
 Hoyle F., Vogeley M. S., Pan D., 2012, *MNRAS*, 426, 3041  
 Kirshner R. P., Oemler A., Jr., Schechter P. L., Shectman S. A., 1981, *ApJ*, 248, L57  
 Krause E., Chang T.-C., Doré O., Umetsu K., 2013, *ApJ*, 762, L20  
 Lavaux G., Wandelt B. D., 2010, *MNRAS*, 403, 1392  
 Lavaux G., Wandelt B. D., 2012, *ApJ*, 754, 109  
 Laureijs R., et al., 2011, *arXiv*, arXiv:1110.3193  
 Melchior P., Sutter P. M., Sheldon E. S., Krause E., Wandelt B. D., 2013, *arXiv*, arXiv:1309.2045  
 Nadathur S., Hotchkiss S., 2013, *arXiv*, arXiv:1310.2791  
 Neyrinck M. C., 2008, *MNRAS*, 386, 2101  
 Pan D. C., Vogeley M. S., Hoyle F., Choi Y.-Y., Park C., 2012, *MNRAS*, 421, 926  
 Park D., Lee J., 2007, *PhRvL*, 98, 081301  
 Patiri S. G., Prada F., Holtzman J., Klypin A., Betancort-Rijo J., 2006b, *MNRAS*, 372, 1710  
 Platen E., van de Weygaert R., Jones B. J. T., 2007, *MNRAS*, 380, 551  
 Plionis M., Basilakos S., 2002, *MNRAS*, 330, 399  
 Quilis V., 2004, *MNRAS*, 352, 1426  
 Ricciardelli E., Quilis V., Planelles S., 2013, *MNRAS*, 434, 1192  
 Sheth R. K., van de Weygaert R., 2004, *MNRAS*, 350, 517  
 Sutter P. M., Lavaux G., Wandelt B. D., Weinberg D. H., 2012a, *ApJ*, 761, 187  
 Sutter P. M., Lavaux G., Wandelt B. D., Weinberg D. H., 2012b, *ApJ*, 761, 44  
 Sutter P. M., Lavaux G., Wandelt B. D., Hamaus N., Weinberg D. H., Warren M. S., 2013, *arXiv*, arXiv:1309.5087  
 York D. G., et al., 2000, *AJ*, 120, 1579  
 van de Weygaert R., Platen E., 2011, *IJMPS*, 1, 41  
 Varela J., Betancort-Rijo J., Trujillo I., Ricciardelli E., 2012, *ApJ*, 744, 82